



This is a repository copy of *Analysis of 1.2kV GaN polarisation superjunction diode surge current capability*.

White Rose Research Online URL for this paper:

<https://eprints.whiterose.ac.uk/194191/>

Version: Published Version

Article:

Sheikhan, A., Narayanankutty, G., Madathil, S. orcid.org/0000-0001-6832-1300 et al. (3 more authors) (2023) Analysis of 1.2kV GaN polarisation superjunction diode surge current capability. *Japanese Journal of Applied Physics*, 62 (1). 014501. ISSN 0021-4922

<https://doi.org/10.35848/1347-4065/aca853>

Reuse

This article is distributed under the terms of the Creative Commons Attribution (CC BY) licence. This licence allows you to distribute, remix, tweak, and build upon the work, even commercially, as long as you credit the authors for the original work. More information and the full terms of the licence here:

<https://creativecommons.org/licenses/>

Takedown

If you consider content in White Rose Research Online to be in breach of UK law, please notify us by emailing eprints@whiterose.ac.uk including the URL of the record and the reason for the withdrawal request.



eprints@whiterose.ac.uk
<https://eprints.whiterose.ac.uk/>

REGULAR PAPER • OPEN ACCESS

Analysis of 1.2 kV GaN polarisation superjunction diode surge current capability

To cite this article: Alireza Sheikhan *et al* 2023 *Jpn. J. Appl. Phys.* **62** 014501


View the [article online](#) for updates and enhancements.

You may also like

- [Improved theoretical minimum of the specific on-resistance of a superjunction](#)
K Akshay and Shreepad Karmalkar
- [A superjunction structure using high-k insulator for power devices: theory and optimization](#)
Huang Mingmin, , Chen Xingbi et al.
- [Practical superjunction MOSFET device performance under given process thermal cycles](#)
Hanmei Zhong, Yung C Liang, Ganesh S Samudra et al.



Analysis of 1.2 kV GaN polarisation superjunction diode surge current capability

Alireza Sheikhan^{1*} , Gopika Narayanankutty¹, E. M. Sankara Narayanan¹, Hiroji Kawai², Shuichi Yagi², and Hironobu Narui²

¹Department of Electronic and Electrical Engineering, The University of Sheffield, Sheffield, United Kingdom

²Powdec K.K., Oyama, Tochigi, Japan

*E-mail: asheikhan1@sheffield.ac.uk

Received August 22, 2022; revised November 10, 2022; accepted December 1, 2022; published online January 9, 2023

The surge current capability of power diodes is one of the essential parameters that needs to be considered for high power density operations in power electronic applications. Gallium Nitride (GaN) is emerging as the next generation of power semiconductor devices due to its superior material characteristics. This work presents the device working principle, characteristics, and the surge capability of 1200 V GaN polarisation superjunction (PSJ) hybrid diodes. The experimental results show that the GaN PSJ diode can withstand a surge current of 60 A which is around 8 times its rated current and a surge energy of 5.4 J. Additionally, despite having a merged PiN and Schottky structure, no bipolar current flow due to the activation of p-doped GaN can be observed until breakdown. This can also be confirmed through the device forward characteristic which shows a unique saturation behaviour at about 76 A without any bipolar region. © 2023 The Author(s). Published on behalf of The Japan Society of Applied Physics by IOP Publishing Ltd

1. Introduction

Gallium Nitride (GaN) is a promising choice for the next generation of power semiconductor devices. The first GaN on sapphire high electron mobility transistor (HEMT) was introduced in 1993.¹⁾ Currently, majority of GaN devices incorporate lateral configurations. Such structures, due to the polarisation properties, benefit from high-density and high mobility of electrons resulting in excellent on-state performance such as low resistance. In recent years, GaN-based devices have gained a significant popularity in lighting, power and radio-frequency applications. GaN hybrid Schottky PiN diodes, due to the wide bandgap of 3.45 eV, can achieve much higher breakdown voltages while offering lower on-state resistances in comparison with conventional silicon-based diodes.²⁻⁷⁾ Additionally, these devices can operate at higher switching speeds enabling the use of smaller magnetic components and operation at higher power densities.²⁾ To go beyond the inherent 1D material limit between the area-specific on-state resistance and breakdown voltage, the concept of superjunction (SJ)^{8,9)} or conductivity modulation schemes are traditionally implemented for silicon (Si) field effect transistors or bipolar devices respectively. In a silicon device, superjunction is achieved by precisely matching the doped charges of p-type and n-type pillars.⁹⁻¹²⁾ Similarly, one of the recent advancements in III-N technologies is the achievement of polarisation based superjunction (PSJ) via double hetero-interfaces (such as GaN/AlGaIn/GaN) to achieve an even distribution of electric field in the drift region to strengthen the reverse blocking capability for a given drift length.^{4,13-17)} Despite works highlighting the advantages of GaN PSJ heterostructure field effect transistors and diodes,¹⁸⁾ and their basic working principles,¹¹⁾ their surge capabilities have not been reported previously. One of the key parameters of power diodes is their surge current capability which is a requirement in cases such as fault occurrences within a system or inrush current during starting phase.¹⁹⁾ The diode must withstand the excess

current over its rating over a short period of time and consequently, it is regarded as a reliability factor.^{20,21)} Therefore, it is necessary to understand their behaviour when subjected to high current stress. Many studies were done to address the surge capability of power diodes in the past decades focusing on silicon and silicon carbide (SiC) devices.²²⁻²⁷⁾ Various reports show that the merged PiN Schottky (MPS) structure improves the surge current capability in SiC devices while reducing the stress due to the field at the Schottky interface resulting in higher blocking voltage.^{24,28,29)} This paper presents the device characteristics of 1.2 kV GaN PSJ diodes fabricated on Sapphire substrate and investigates the surge current capability and the maximum surge current and energy that the device can handle before failure. Additionally, the effect of surge current on the device is discussed and the device characteristics are measured and illustrated.

2. Device structure and characteristics

2.1. Structure and working mechanism

Conventionally, doping methods are used for controlling the number of mobile carriers to control the material conductivity. However, GaN PSJ devices benefit from co-existence of high-density two-dimensional hole gas (2DHG) and two-dimensional electron gas (2DEG) formed at the respective heterostructure interfaces, GaN/AlGaIn/GaN, due to the piezoelectric and polarisation effects. The device uses the concept of polarisation charge balance to achieve a flat distribution of electric field resulting in an enhanced blocking voltage capability.³⁾ Figure 1(a) shows the top view of a 1.2 kV GaN PSJ diode bare die. The number of fingers connected to the anode and cathode terminals are 47 and 48 respectively with a length of 2.39 mm. The cross-sectional view of the device is depicted in Fig. 1(b) highlighting the device's physical dimensions and material parameters. The 2DEG and 2DHG under thermal equilibrium have a density of $1.2\text{E}13\text{ cm}^{-2}$ and $6.12\text{E}12\text{ cm}^{-2}$ respectively. The p-GaN is doped with Magnesium with a doping density of $5\text{E}19$



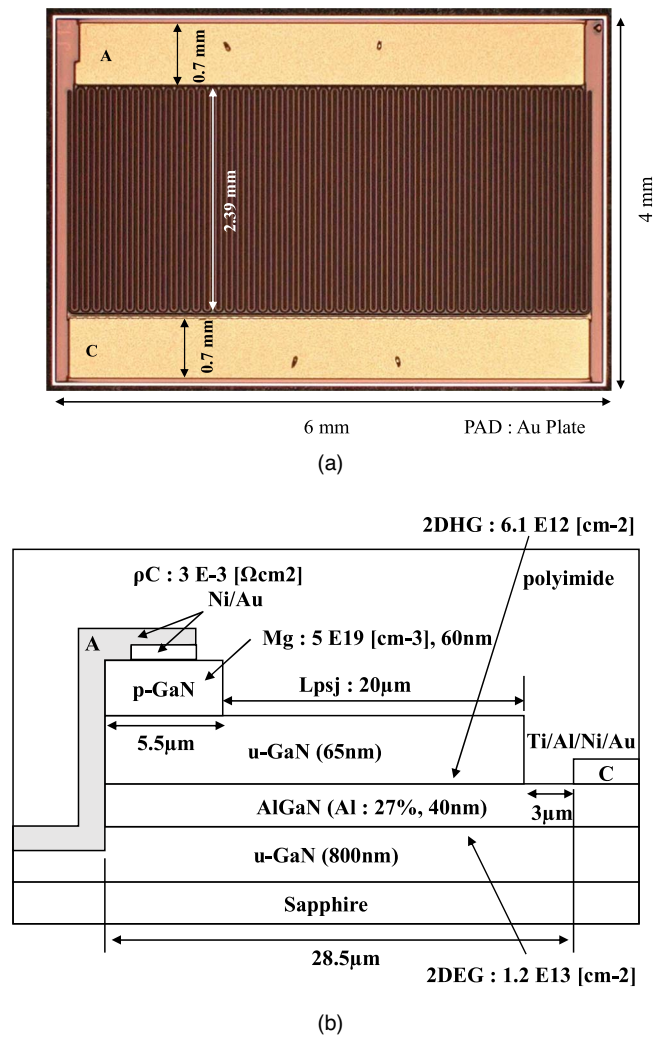


Fig. 1. (Color online) (a) Top view of a 1.2 kV GaN PSJ diode chip and (b) the simplified cross-sectional view of the diode structure. The anode and cathode are marked as “A” and “C” respectively.

cm^{-3} and the Al concentration in the AlGaIn layer is fixed at 27%.

The specific contact resistance of the p-GaN ohmic contact (ρ_C) is $3\text{E-}3 \Omega\text{cm}^2$. The drift region length (L_{PSJ}) is $20 \mu\text{m}$ which determines the device voltage blocking capability. The device is capable of blocking 1.2 kV with a typical breakdown voltage of $\sim 2\text{ kV}$. In reverse blocking mode, the polarisation charges in the 2DHG and 2DEG are removed through the anode (A) and cathode (C) respectively.¹⁸⁾ The absence of polarisation charges results in an even distribution of electric field enabling extremely high reverse voltage blocking capability superior to conventional GaN HEMTs.¹¹⁾ In forward conduction mode, once the voltage across the device (V_{AC}) exceeds the Schottky barrier potential of $\sim 1\text{ V}$, the current flows via the dense two-dimensional electron gas from the anode to the cathode. Due to the high bipolar on-set voltage of 3.4 V of the anode junction at room temperature and the very low resistance offered by the 2DEG beneath the 2DHG region, the PiN diode does not turn on under normal conditions.

2.2. Forward characteristics

The forward characteristics of the GaN PSJ diode have been measured at different temperatures as shown in Fig. 2. The extended forward characteristics are shown in Fig. 3

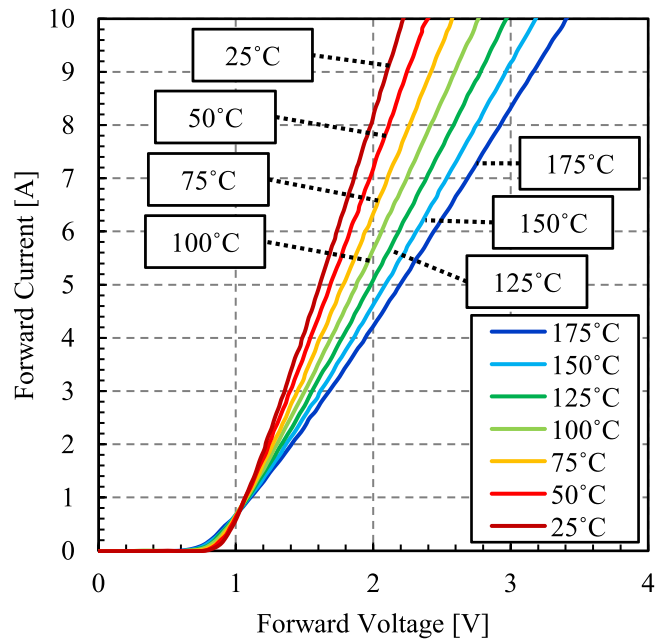


Fig. 2. (Color online) Forward (I - V) characteristics of the GaN PSJ diode at different temperatures. The pulse width is $250 \mu\text{s}$.

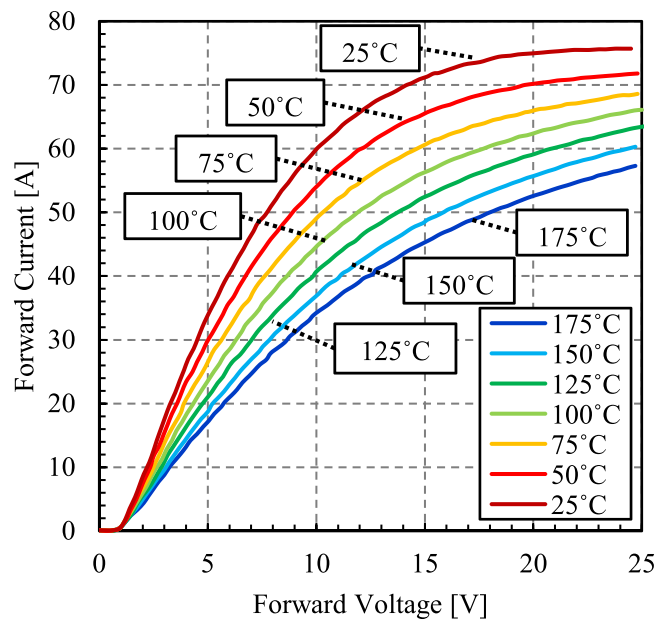


Fig. 3. (Color online) Extended forward (I - V) characteristics of the GaN PSJ diode at different temperatures. The pulse width is $250 \mu\text{s}$. The GaN PSJ diode reaches a saturation at 76 A at 25°C .

highlighting the device's current saturation at about 76 A at 25°C . The forward I - V characterisations are carried out in pulse mode with $250 \mu\text{s}$ pulse width and 160 ms pulse period resulting in a duty cycle of 0.15625 %. The following parameters are extracted from the forward characteristics; The diode forward voltage V_{F0} and slope resistance R_{slope} at 25°C are 0.9 V and 125 m Ω respectively. The device has a forward voltage V_{Fwd} of 1.6 V at 5 A at 25°C .

The device's forward voltage and the slope resistance increase to 2.2 V and 239 m Ω respectively at 5 A at 175°C .

Despite having a merged PiN and Schottky configuration, the GaN PSJ diode behaves like a pure Schottky diode without a bipolar mode of operation. This is entirely due to the low resistance of the 2DEG beneath the 2DHG region,

ultra-short lifetime of holes and high bipolar on-set voltage. Consequently, the diode shows saturation at a current of about 76 A at room temperature. However, in extreme surge current conditions, the bipolar mode can be triggered which results in sudden injection of holes leading to device failure. This condition will be discussed in Sect. 4 of this paper.

2.3. Junction capacitance characteristic

The device capacitance versus reverse voltage has been measured at a frequency of 1 MHz as shown in Fig. 4. The device capacitance is 34 pf at 1200 V.

Two humps can clearly be seen in the measured C–V characteristic shown in Fig. 4, which are attributed to the two-step depletion process due to the 2DEG and 2DHG.¹⁸⁾ It has been previously reported that while the PSJ diodes exhibit a two-step depletion, conventional GaN diodes do not have a second hump due to the lack of 2DHG.¹⁸⁾ As shown in Fig. 4, the depletion process happens under the Schottky region of the anode ending at $V_{CA} \sim 3.3$ V followed by the second depletion under the ohmic region ending at $V_{CA} \sim 5.5$ V.

2.4. Reverse recovery measurements

Conventional PiN diodes exhibit a reverse current flow during the transition from the forward conduction to the reverse blocking state. During this time, minority carriers are swept out from the junction resulting in a reverse current flow known as reverse recovery. But Schottky diodes, due to the lack of minority carriers, show very little to effectively zero reverse recovery current flow.³⁰⁾ However, due to the capacitively stored charges due to the junction capacitance of the diode, a small reverse recovery can be observed in the switching waveform.

The typical reverse recovery waveform and the test circuit are presented in Fig. 5. The shaded area which is the integration of the current waveform during the reverse recovery time (t_{rr}) represents the total recovered charges (Q_{rr}) which can be calculated as follow:

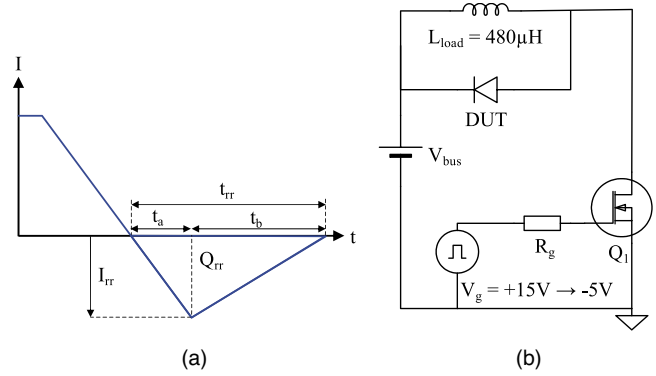


Fig. 5. (Color online) (a) Typical reverse recovery waveform and (b) test circuit for reverse recovery measurement.

$$Q_{rr} = \int_{t_0}^{t_0+t_{rr}} i \cdot dt. \tag{1}$$

The integration is performed from t_0 as soon as the diode current passes zero until the current recovers back, t_{rr} . The diode softness factor is determined by the ratio between the reverse recovery current fall time (t_b) and rise time (t_a):

$$\text{softness factor} = \frac{t_b}{t_a}. \tag{2}$$

When the softness factor is more than 1, the diode has a soft recovery. Otherwise, the term “snappy” is used for softness factors of less than 1. Using the circuit presented in Fig. 5(b) the reverse recovery of the GaN PSJ diode was measured. The current was increased in 1 A step by increasing the voltage (V_{bus}) from 50 to 300 V (50 V steps), and the results were recorded as presented in Fig. 6.

The total reverse recovery charge (Q_{rr}) is 45nC at the current (I_{load}) of 6 A with a peak reverse current (I_{rr}) of -4.35 A at room temperature. The reverse recovery time (t_{rr}) is 20 ns and the diode softness factor is 0.6.

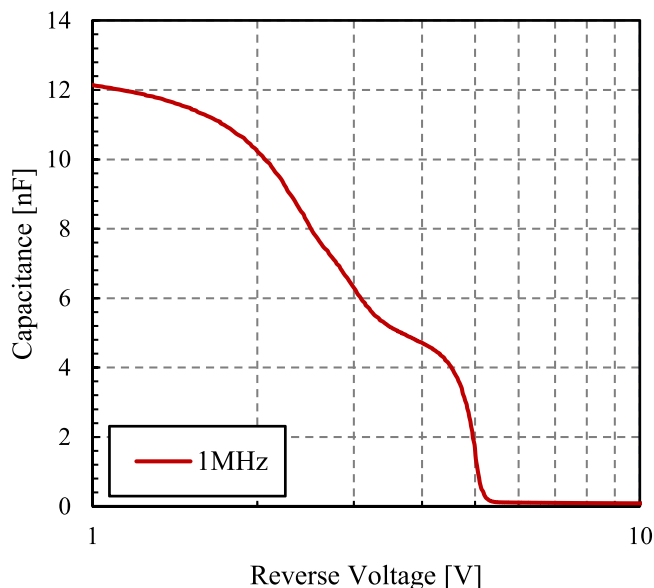


Fig. 4. (Color online) Capacitance versus reverse voltage (C–V) characteristic of the GaN PSJ diode measured at 1 MHz.

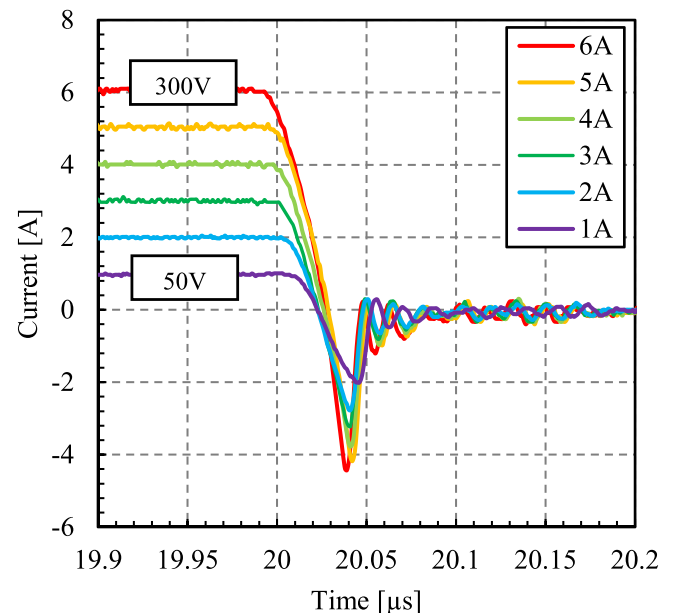


Fig. 6. (Color online) GaN PSJ diode reverse recovery waveforms at various current levels at room temperature.

3. Experimental setup

A dedicated test bench was built for investigating the surge current capability of the GaN PSJ diode as shown in Fig. 7. The setup uses an autotransformer T2 to step down the voltage to control the desired surge current flow through the diode DUT. Further components, including an isolation transformer T1 and input/output fuses are in place for safety measures.

The current flow is controlled by the thyristor Ty1 which is driven by the control circuitry shown in Fig. 8. The circuit is designed to provide a single half sinusoidal pulse with 10 ms pulse width. The control system applies a trigger pulse that is synchronised with the mains (input) 50 Hz frequency to the gate terminal of the thyristor Ty1. Therefore, during the thyristor on-state, a single half sinusoidal wave with the pulse width of 10 ms is passed through the device under test (DUT).

The voltage across the diode has been increased in steps and the corresponding data was captured. In order to analyse the influence of surge current stress on the device, a number of End-of-Lifetime (EOL) criteria and aging mechanisms have been studied including an increase in diode forward voltage drop, a degradation in reverse blocking capability or an increase in reverse leakage current.²⁰⁾ The device forward and reverse characteristics were measured by Tektronix 371B curve tracer and Agilent B1505 power device analyser, respectively, prior to the conduction of the surge current experiment and after every 10 A surge current step.

4. Measurement results and discussion

4.1. Maximum surge current limit

After the initial device characterisation, the experiment has been conducted to determine the maximum surge capability of the GaN PSJ diode. A 10 ms half-sine current pulse was imposed on the device at different current levels. The measured voltage waveforms (across the diode, V_{AC}) at different surge current levels are shown in Fig. 9.

The results show that the diode survived up to 60 A which is nearly 8 times the device-rated current. The maximum deposited surge energy was calculated by the integration of the dissipated power over the 10 ms surge current during the last pulse before failure which corresponds to 5.4 J. At 58.3 A pulse, a secondary voltage peak can be observed which indicates the activation of bipolar operation mode. The corresponding surge current $I-V$ characteristics are shown in Fig. 10.

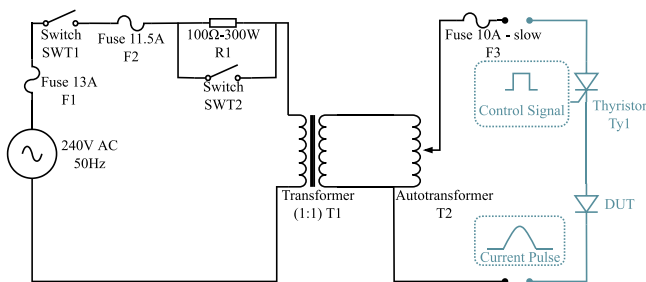


Fig. 7. (Color online) Simplified circuit diagram of the experimental setup. A 10 ms half-sine wave pulse is applied to the DUT when the control signal is triggered.

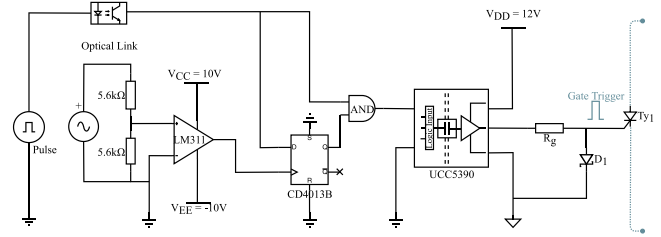


Fig. 8. (Color online) Synchronised pulse generator circuit diagram. The circuit generates a single pulse synchronised with the input frequency.

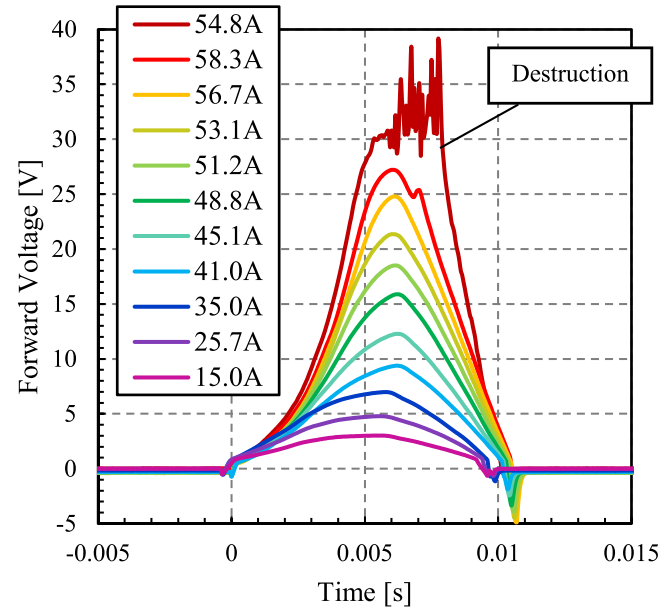


Fig. 9. (Color online) Voltage waveforms (V_{AC}) of the GaN PSJ diode at different surge current conditions.

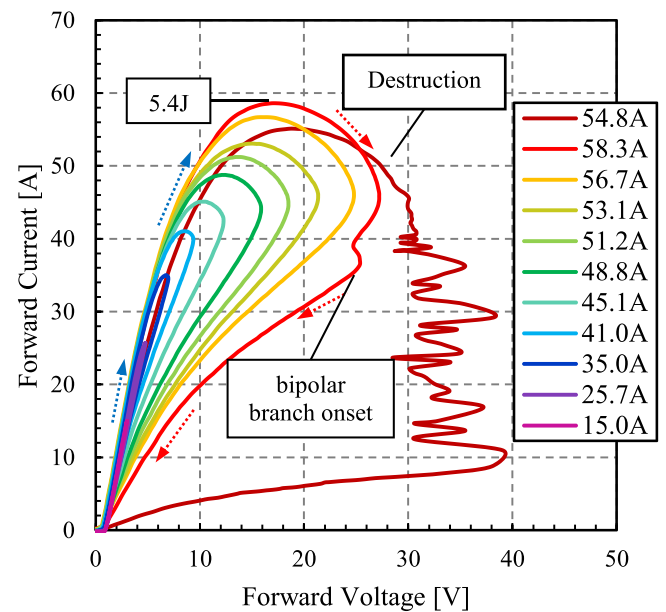


Fig. 10. (Color online) Corresponding $I-V$ curves of the GaN PSJ diode at different surge current conditions. The pulse width is 10 ms.

A rising and a falling branch can be clearly seen due to the influence of temperature. The device's positive temperature coefficient causes the current in the falling (return) branch to be lower with a higher forward voltage drop. At 58.3 A pulse, it can be observed that there is a sudden increase in forward

voltage in the return branch that corresponds to the triggering of the bipolar regime at ~ 25 V. Subsequently, the inrush of minority carriers (holes) from the p-GaN region due to activation of bipolar mode leads to the device degradation. The bipolar operation is only observed in the return/falling branch which is due to the temperature dependency of the bipolar on-set voltage, which reduces due to self-heating. Meanwhile, in the rising branch at 25 V, no sign can be seen which indicates the likely thermal influence on the device. Due to the generated heat during the surge current event, the on-set voltage of the PiN diode reduces along with the decreased mobility of the 2DEG beneath the p-GaN region causing higher resistance and a larger voltage drop across the PiN diode that triggers the bipolar current flow and the injection of minority carriers. On the other hand, in the extended I - V characteristics (as shown previously in Fig. 3), the bipolar operation is not present due to the short pulse width of $250 \mu\text{s}$ which does not contribute to a noticeable temperature rise. The destruction happened at about 60 A where the device failed due to high-level of surge current. During the last surge current pulse (54.8 A) before the destruction, the rising branch shows a significant degradation in current due to the partial damage from the previous surge current pulse of 58.3 A.

4.2. Influence of surge current on device and aging mechanism

The device's static characteristics were monitored for changes in on-state performance, reverse leakage current and blocking voltage capability. The device was characterised prior to the test and during the test after every 10 A increase in the surge current. The forward characteristics of the device are shown in Fig. 11. The dashed line highlights the last measured result (after 51 A surge current pulse) while the solid line represents the initial measurement prior to the test.

A minor shift in the forward current can be observed particularly at higher forward voltage. Similarly, the reverse

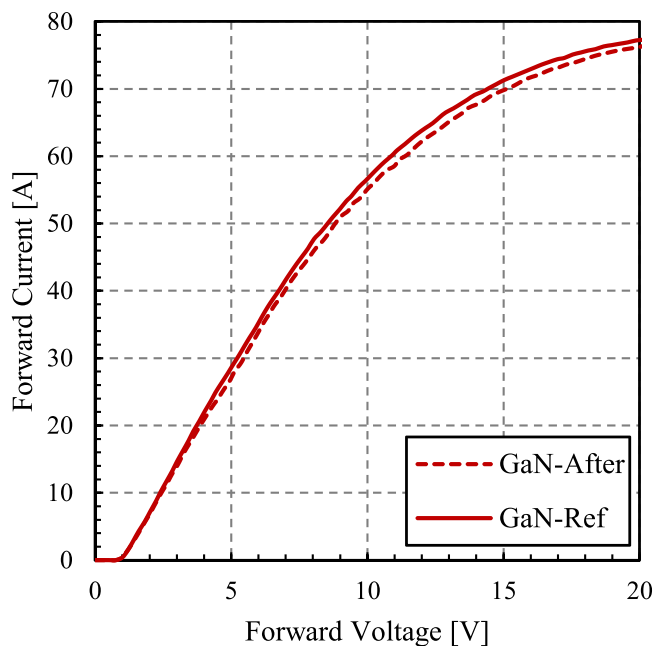


Fig. 11. (Color online) Forward characteristics of the GaN PSJ diode prior to the test (solid line) and before the failure after the 51 A surge current pulse (dashed line).

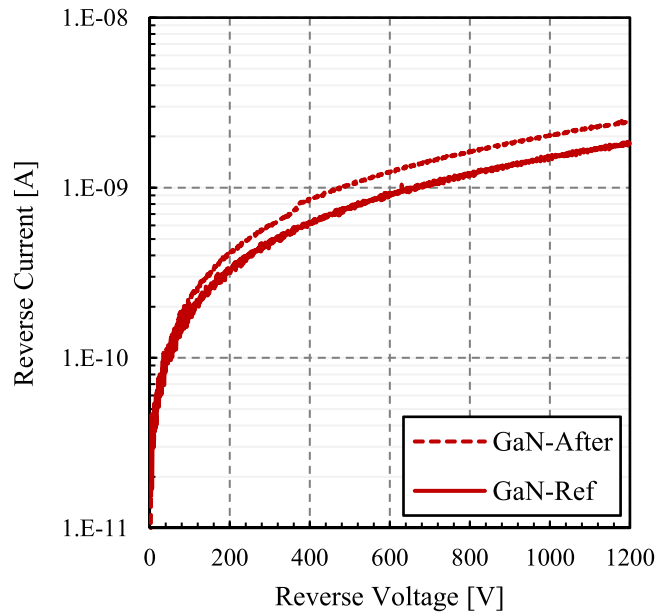


Fig. 12. (Color online) Reverse leakage current of the GaN PSJ diode. The measurements were carried out prior to the test (solid line) and before the failure (dashed line) after the 51 A surge current pulse.

characteristics are illustrated in Fig. 12 comparing the reverse leakage current of the device before the failure (dashed line, after 51 A surge current pulse) to the initial measurement (solid line, before the test). While the device managed to maintain its rated blocking voltage capability, a slight increase in leakage current can be observed.

Reverse voltage blocking capability and leakage current were observed to have minor degradation before device failure.

4.3. Failure mechanism and analysis

At the surge current of nearly 60 A, the GaN PSJ diode broke down due to the high-level of current. The device failed in the open circuit. The failure region can be observed in Fig. 13.

As can be seen, the device failure region can be observed on the anode fingers near the cathode terminal uniformly distributed across the device. The possible reason for this can be attributed to the triggering/activation of the p-GaN contact near the anode region where the damage can be seen. The activation of the p-GaN region results in a significant number

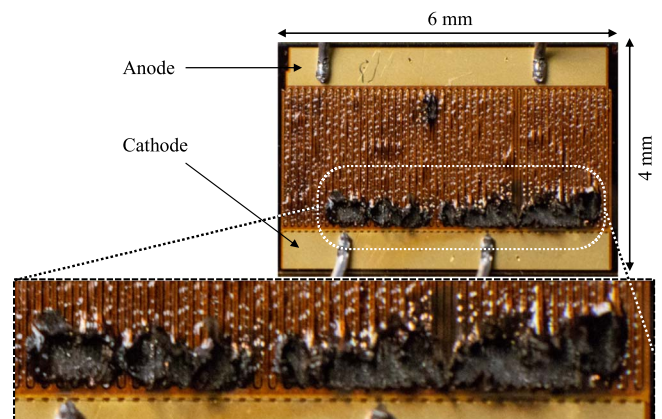


Fig. 13. (Color online) GaN PSJ diode after the failure. The black regions are the burnt-out failure points.

of high-energy minority carriers to be injected into the device which could result in lattice damage and device failure.

5. Conclusion

This work presented the device characteristics and the surge current capability of the 1.2 kV GaN PSJ diode for the first time. As can be seen, the GaN diode demonstrated a surge capability of nearly 8 times its rated current. The total surge energy before failure was measured to be 5.4 J. Due to the significant amount of surge current stress on the device and dissipated power, failure can be seen near the cathode region of the device. However, the damaged areas are within the anode fingers and uniformly distributed across the device. The failure mechanism is attributed to the activation of the PiN region which results in the sudden injection of minority carriers into the device and device failure. In terms of degradation, no significant changes were seen in advance of the failure. The results show that GaN PSJ diodes can be highly cost-effective and reliable for high frequency, high-efficiency power electronic designs.

ORCID iDs

Alireza Sheikhan  <https://orcid.org/https://orcid.org/0000-0002-2207-1593>

- 1) M. A. Khan, A. Bhattarai, J. N. Kuznia, and D. T. Olson, *Appl. Phys. Lett.* **63**, 1214 (1993).
- 2) H. Amano et al., *J. Phys. D: Appl. Phys.* **51**, 163001 (2018).
- 3) A. Nakajima, K. Adachi, M. Shimizu, and H. Okumura, *Appl. Phys. Lett.* **89**, 193501 (2006).
- 4) A. Nakajima, Y. Sumida, M. H. Dhyani, H. Kawai, and E. M. S. Narayanan, *IEEE Electron Device Lett.* **32**, 542 (2011).
- 5) B. J. Baliga, *Semicond. Sci. Technol.* **28**, 074011 (2013).
- 6) W. Saito, T. Nitta, Y. Kakiuchi, Y. Saito, K. Tsuda, I. Omura, and M. Yamaguchi, *IEEE Trans. Electron Devices* **54**, 1825 (2007).
- 7) N.-Q. Zhang, S. Keller, G. Parish, S. Heikman, S. P. DenBaars, and U. K. Mishra, *IEEE Electron Device Lett.* **21**, 421 (2000).
- 8) T. Fujihira, *Jpn. J. Appl. Phys.* **36**, 6254 (1997).
- 9) G. Deboy, N. Marz, J.-P. Stengl, H. Strack, J. Tihanyi, and H. Weber, *IEDM Tech. Dig.*, 1998, p. 683.
- 10) S. Shirota and S. Kaneda, *J. Appl. Phys.* **49**, 6012 (1978).
- 11) H. Kawai, S. Yagi, S. Hirata, F. Nakamura, T. Saito, Y. Kamiyama, M. Yamamoto, H. Amano, V. Unni, and E. M. S. Narayanan, *Phys. Status Solidi a* **214**, 1600834 (2017).
- 12) D. J. Coe, US Patent 4754310 (1988).
- 13) K. Nomoto, B. Song, Z. Hu, M. Zhu, M. Qi, N. Kaneda, T. Mishima, T. Nakamura, D. Jena, and H. G. Xing, *IEEE Electron Device Lett.* **37**, 161 (2016).
- 14) A. Nakajima, Y. Sumida, M. H. Dhyani, H. Kawai, and E. M. S. Narayanan, *Appl. Phys. Express* **3**, 121004 (2010).
- 15) A. Nakajima, M. H. Dhyani, E. M. S. Narayanan, Y. Sumida, and H. Kawai, *Proc. Int. Symp. Power Semiconductor Devices and ICs*, 2011, p. 280.
- 16) A. Nakajima, V. Unni, K. G. Menon, M. H. Dhyani, E. M. S. Narayanan, Y. Sumida, and H. Kawai, *Proc. Int. Symp. Power Semiconductor Devices and ICs*, 2012, p. 265.
- 17) A. Nakajima, K. Adachi, M. Shimizu, and H. Okumura, *Appl. Phys. Lett.* **89**, 193501 (2006).
- 18) V. Unni, H. Long, M. Sweet, A. Balachandran, E. M. S. Narayanan, A. Nakajima, and H. Kawai, *Proc. Int. Symp. Power Semiconductor Devices and ICs*, 2014, p. 245.
- 19) S. Fichtner, J. Lutz, T. Basler, R. Rupp, and R. Gerlach, *Proc. Int. Conf. on Integrated Power Electronics Systems*, 2014, pp. 1–5.
- 20) S. Palanisamy, J. Kowalsky, J. Lutz, T. Basler, R. Rupp, and J. Moazzami-Fallah, *Proc. Int. Symp. Power Semiconductor Devices and ICs*, 2018, p. 367.
- 21) B. Heinze, J. Lutz, M. Neumeister, R. Rupp, and M. Holz, *Proc. Int. Symp. Power Semiconductor Devices and ICs*, 2008, p. 245.
- 22) D. Silber and M. J. Robertson, *Solid-State Electronics* **16**, 1337 (1973).
- 23) V. Banu, M. Berthou, J. Montserrat, X. Jorda, and P. Godignon, *Rom. J. Inf. Sci. Technol.* **20**, 369 (2017).
- 24) R. Rupp, M. Treu, S. Voss, F. Björk, and T. Reimann, *Proc. Int. Symp. Power Semiconductor Devices and ICs*, 2006, p. 1.
- 25) J. Millan, V. Banu, P. Brosselard, X. Jorda, A. Perez-Tomas, and P. Godignon, *Int. Semiconductor Conf.*, 2008, pp. 53–59.
- 26) V. Banu, X. Jorda, J. Montserrat, P. Godignon, J. Millan, and P. Brosselard, *Proc. Int. Symp. Power Semiconductor Devices and ICs*, 2009, p. 267.
- 27) S. Palanisamy, S. Fichtner, J. Lutz, T. Basler, and R. Rupp, *Proc. Int. Symp. Power Semiconductor Devices and ICs*, 2016, p. 235.
- 28) F. Dahlquist, J. O. Svedberg, C. M. Zetterling, M. Östling, B. Breitholtz, and H. Lendenmann, *Mater. Sci. Forum* **338-342**, 1179 (2000).
- 29) F. Bjoerk, J. Hancock, M. Treu, R. Rupp, and T. Reimann, *Appl. Power Electronic Conf. and Expo.*, 2006, p. 170.
- 30) R. Singh, S.-H. Ryu, J. W. Palmour, A. R. Hefner, and J. Lai, *Proc. Int. Symp. Power Semiconductor Devices and ICs2000p*. 101.